Ultrasound in Medicine & Biology 52 (2026) 1973–1984

Contents lists available at ScienceDirect

Ultrasound in Medicine & Biology

journal homepage: www.elsevier.com/locate/ultrasmedbio

Original Contribution

Boiling Histotripsy *Ex Vivo* in Human Liver Metastases of Various Origin

Ekaterina Ponomarchuk[a,*], Sergey Tsysar[a], Oleg Sapozhnikov[a], Anastasia Kvashennikova[a], Polina Pestova[a], Daria Chupova[a], Liliya Papikyan[a], Fedor Nartov[a], Anastasia Bashmashnikova[a], Alexey Kadrev[b,c], Armais Kamalov[b], Tatiana Sotnikova[d], Anton Grachalov[e], Ivan Ivashov[e], Tatiana Khorobrykh[e], Natalia Danilova[b], Pavel Malkov[b], Sergey Buravkov[f], Vera Khokhlova[a]

[a] *Physics Faculty, Lomonosov Moscow State University, Moscow, Russia*
[b] *Lomonosov Moscow State University Clinic, Lomonosov Moscow State University, Moscow, Russia*
[c] *Diagnostic Ultrasound Division, Russian Medical Academy of Continuous Professional Education, Moscow, Russia*
[d] *Moscow Department of Healthcare, Davydovsky Clinical Hospital, Moscow, Russia*
[e] *Department of Faculty Surgery No. 2, Sechenov First Moscow State Medical University, Moscow, Russia*
[f] *Faculty of Fundamental Medicine, Lomonosov Moscow State University, Moscow, Russia*

ARTICLE INFO

Keywords:
HIFU
Boiling histotripsy
Non-invasive surgery
Liver cancer
Liver metastases

ABSTRACT

Objective: Given the high incidence rate of secondary liver tumors and limitations of the existing treatment options, boiling histotripsy (BH) may provide an incisionless, non-ionizing, ultrasound-guided approach for the mechanical ablation of liver metastases using pulsed high-intensity focused ultrasound waves with shock fronts. This pilot *ex vivo* study investigated the feasibility of BH for mechanical disintegration of human liver metastases with respect to tumor origin, stiffness, and prior anti-tumor treatment.

Methods: Eighteen human liver metastases were collected *via* surgical resection or rapid autopsy from anonymized patients aged 39–85 y (median: 68) with confirmed colorectal, gastric, breast, or skin (cutaneous melanoma) cancers, with or without prior targeted therapy or radiation therapy. The Young's moduli of the tumors and adjacent liver tissue were measured using shear wave elastography. BH was then applied to nodes of a volumetric grid (1 −4 layers, $3 \times 3 - 5 \times 5$ points per layer, and 1-mm spacing) at 25–200 pulses per point (1-ms pulses and 1% duty cycle) using a 9-ring 2-MHz annular array under real-time ultrasound guidance. Histological analysis of the treatment outcomes was performed with H&E and Masson's trichrome stains; scanning and transmission electron microscopy were employed for ultrastructural analysis of the fragmented tissue.

Results: Liver metastases were significantly stiffer than the adjacent liver parenchyma (44 ± 17 kPa vs. 9.3 ± 3.9 kPa; $p < 9 \times 10^{-5}$) regardless of tumor origin; these findings are consistent with clinically relevant Young's modulus values reported in prior *in vivo* studies. In metastases with spontaneous or prior therapy-induced necrosis, all investigated BH protocols successfully disintegrated the planned volumes; the highest treatment rate of 54 mm^3/min was achieved using 75 pulses per point. In metastases with therapy-induced fibrosis, complete disintegration of target volumes was achieved only at 200 pulses per point (treatment rate: 14 mm^3/min), whereas lower pulse numbers resulted in the selective fragmentation of non-fibrotic tumor components. Electron microscopy confirmed mechanical disintegration of the tumor tissue down to the subcellular level.

Conclusion: BH enables non-invasive mechanical ablation of human liver metastases across multiple primary origins. The treatment process can be accelerated by reducing pulse numbers for non-fibrotic or necrotic tumors; however, fibrotic tumors require higher number of BH pulses for complete disintegration. These findings support the use of BH as a potential modality for managing liver metastases, whether applied as a standalone procedure, a neoadjuvant strategy, or following anti-tumor therapy to ensure complete removal of the residual tumor burden.

Introduction

Given the high incidence of primary and metastatic liver tumors and the limitations of current therapies, there is an urgent clinical need for novel, accessible, and safe local ablation methods. These modalities should be applicable to a broader patient population than is currently eligible for existing treatment options. In clinical practice, metastatic liver malignancies are more prevalent than primary liver cancer, occurring in approximately 25% of all cancer patients and 50% of those diagnosed with colorectal cancer. Notably, colorectal cancer is the third

* Corresponding author. Physics Faculty, Lomonosov Moscow State University, Leninskie Gory, 1-2, Moscow, Russia
E-mail address: msu.ekaterina.ponomarchuk@gmail.com (E. Ponomarchuk).

https://doi.org/10.1016/j.ultrasmedbio.2026.05.017
Received 4 December 2025; Revised 7 May 2026; Accepted 14 May 2026

most common malignancy and the second leading cause of cancer-related mortality worldwide [1–3]. The most common primary sites of liver metastases are breast cancer in younger women and colorectal cancer in younger men, while other primaries include pancreatic, lung, gastric, esophageal, small intestine cancers, and melanoma [4]. In nearly 70%–80% of cases, metastases are confined exclusively to the liver, making their effective treatment a critical determinant of patient survival [5].

The current standard of care for liver tumor management is surgical resection. However, it is feasible in fewer than 20% of patients due to tumor burden, multifocality, or underlying comorbidities. Furthermore, as an invasive procedure, surgery carries inherent risks such as infection, bleeding, high recurrence rates, and other complications [1,3]. Other therapeutic options include systemic drug therapy—such as chemotherapy, immunotherapy, and targeted therapy—which often lacks efficacy and is associated with systemic toxicity [1,6–9].

The concept of treating limited metastatic disease—termed oligometastases—is gaining popularity supported by evidence that aggressive local control of metastatic sites can significantly improve treatment outcomes [10,11]. Minimally invasive local ablation techniques such as cryoablation, laser ablation, radiofrequency ablation (RFA), microwave ablation, and trans-arterial chemoembolization (TACE) are current alternatives for unresectable tumors and surgically or therapeutically ineligible patients. While these modalities are well-established in oncology, they have inherent limitations: their efficacy is typically restricted to smaller tumors (<3–5 cm), and thermal techniques can be compromised by the heat-sink effect of adjacent large vessels, increasing the risk of local recurrence [12–14]. Consequently, there is a strong clinical need to develop novel non-invasive approaches for local ablation of liver malignancies that would offer greater efficacy and broader patient eligibility.

High-intensity focused ultrasound (HIFU) is emerging as a fully non-invasive, non-ionizing thermal ablation modality for diverse clinical applications, including local tumor ablation [15,16]. The HIFU approach relies on transcutaneous ultrasound irradiation of the target site for several seconds. Absorption of the ultrasound energy by tissue within the focal region results in tissue heating and subsequent thermal necrosis [15–17]. A systematic review reported complete tumor ablation in 55% of 940 liver tumor cases treated with HIFU alone, rising to 66% when combined with TACE, RFA, or percutaneous ethanol injection [18]. However, the precision of such thermal HIFU ablation is limited by heat diffusion from the focal zone, which can cause collateral damage to healthy tissues or undertreatment of the target zone due to microvascular perfusion effects. In addition, HIFU treatment near major vessels is particularly challenging due to the pronounced heat-sink effect, which not only compromises ablation efficacy but also elevates the risk of vascular complications such as adhesions and vascular thrombosis. Due to prolonged ultrasound exposure, the most frequent adverse effect of HIFU liver ablation is skin and subcutaneous tissue burn, occurring in approximately 24% of treatments [19]. Moreover, real-time visualization of purely thermal HIFU treatment with the use of diagnostic ultrasound modalities is limited, and reliable thermometry requires costly MRI equipment. Furthermore, heat-induced tissue necrosis following HIFU ablation takes a long time to be resorbed through immune-mediated mechanisms.

A newer HIFU-based approach termed *histotripsy* enables mechanical tissue ablation through the use of short high-amplitude pulses delivered at low duty cycle to prevent heat accumulation, as opposed to thermal tissue coagulation produced by long quasi-harmonic exposures [20,21]. Mechanical tissue ablation in histotripsy is achieved through the initiation of bubble activity within the focal zone, resulting in tissue liquefaction into an acellular suspension. Consequently, the focal region is clearly visible on diagnostic ultrasound as a hyperechoic zone during the treatment due to bubble activity, transitioning to hypoechoic appearance post-treatment, once the tissue is liquefied and devoid of ultrasound scatterers. This distinct visual feedback eliminates the necessity for MR-thermometry. Histotripsy methods are actively being investigated for numerous clinical applications including the treatment of liver tumors [22].

One of the histotripsy types termed *cavitation histotripsy* (CH) relies on initiation of dense cavitation clouds in the focal area. CH employs a sequence of either single-cycle HIFU pulses (1–2 μs) with very high peak rarefactional pressures (>27 MPa) exceeding the intrinsic threshold for bubble formation in the medium, or microsecond-long HIFU pulses (5–25 μs) with shock fronts at the focus and 15–25 MPa peak rarefactional pressures [23]. This second mechanism relies on the generation of a cavitation cloud through incidental bubble formation and the subsequent scattering of shock fronts at tissue-bubble interfaces. CH has recently been approved by the US Federal Food and Drug Administration (FDA) for mechanical ablation of liver tumors and is currently being investigated in the ongoing clinical trial for colorectal cancer metastases in liver [24,25]. However, generating the extremely high negative pressures essential for the CH approach requires the use of large transducers, which restricts the portion of liver available for the treatment and narrows patient selection criteria [26].

An alternative histotripsy approach termed *boiling histotripsy* (BH) produces mechanical tissue ablation at lower acoustic pressures and with more compact transducers than CH [27,28]. The BH approach relies on sequences of millisecond-long HIFU pulses with shock fronts that rapidly heat tissue and induce localized boiling at the focus within each pulse. The interaction of subsequent shocks of the pulse with the resulting vapor bubble interface liquefies tissue through a combination of mechanisms including pre-focal cavitation, acoustic atomization, and the "microfountain" effect. Similar to CH, collateral thermal damage of tissue is prevented by maintaining a low duty cycle. Despite the use of more compact transducers, BH-induced regions of tissue disintegration (hereinafter referred to as *lesions*) are typically larger than those produced by CH. This suggests the potential utility of BH for treating larger targets within a shorter timeframe [29].

BH has been shown to be feasible for non-invasive, non-thermal ablation of both benign and malignant tumors in prostate, uterus, breast, and kidney in *ex vivo* human tissues, and for generating lesions in the liver and kidney in animal models *in vivo* [30–36]. In the context of liver treatment, BH has been successfully applied for liquefaction of target volumes in healthy liver tissue across various exposure parameters in both *ex vivo* and *in vivo* animal studies [37–41]. Post-treatment liver healing was characterized by regeneration of normal hepatocytes and vasculature, with no evidence of progressive fibrosis [41]. Small animal studies have also demonstrated the potential of BH for treating liver fibrosis and achieving tissue decellularization for further intra-hepatic delivery of healthy liver cells [42,43]. Beyond direct tissue disintegration, another promising feature of histotripsy is its potential to facilitate liquid biopsy and immunomodulation by releasing tumor biomarkers into the bloodstream, triggering immune cell infiltration of both treated and untreated tumors, and promoting sensitization to immunotherapeutic drugs [44–50].

While BH has been validated for the disintegration of healthy liver tissue in animal models, its feasibility for the mechanical ablation of human liver metastases has not yet been investigated. Such metastases are highly heterogeneous, often characterized by varying stromal density and zones of necrosis or fibrosis [51]. Therefore, the aim of this pilot *ex vivo* study was to evaluate the potential of BH for the mechanical ablation of human liver metastases, assessing treatment efficacy across common tumor origins with respect to tissue stiffness, composition, and prior anti-tumor therapy.

Materials and methods

Tissue sample collection

A total of 18 human liver metastasis samples (Table 1) were collected *via* surgical resection or rapid autopsy (<24 h after death, archive

Table 1
Treatment parameters for volumetric boiling histotripsy in samples of *ex vivo* human liver with metastases of various origin, with, or without prior treatment

Primary cancer and type of metastases	Prior treatment	Gender	Age, y/o	Target volume location	Pulses per point	Sonicated grid of points	Treatment time, min	Average focus depth in tissue, mm
Gastric adenocarcinoma	None	Male	62	Metastasis	50	4 × 4 × 2	2.67	6
				Metastasis	75	4 × 4 × 2	4	6
				Edge[a]	150	4 × 4 × 2	8	8
Gastric poorly differentiated adenocarcinoma	None	Male	68	Edge[a]	50	5 × 5 × 3	6.25	10
Colorectal mucinous adenocarcinoma	None	Male	85	Metastasis	25	5 × 5 × 3	3.13	10
				Edge[a]	25	5 × 5 × 3	3.13	10
				Edge[a]	50	5 × 5 × 3	6.25	10
				Edge[a]	50	5 × 5 × 3	6.25	8
				Liver	50	5 × 5 × 3	6.25	10
Cutaneous melanoma	Radiation therapy + targeted therapy	Female	39	Metastasis	150	5 × 5 × 3	18.75	4
				Metastasis	150	3 × 3 × 1	2.25	5
				Metastasis	150	3 × 3 × 1	2.25	4
				Edge[a]	150	5 × 5 × 1	6.25	5
				Edge[a]	150	4 × 4 × 2	8	8.5
				Liver	150	5 × 5 × 1	6.25	5
Breast adenocarcinoma	Radiation therapy	Female	85	Metastasis	100	5 × 5 × 2	8.33	6
				Metastasis	150	5 × 5 × 4	25	9
				Metastasis	200	5 × 5 × 3	25	8.5

[a] Target volume location "edge" indicates the treatment that was planned to partially cover a metastasis and adjacent liver parenchyma.

material, institutional review board exempt) from five anonymized patients aged 39–85 y (median: 68). Samples of metastases of different primary origins, with or without prior anti-tumor treatment, were included in the study (Table 1).

Four samples were obtained from two gastric cancer patients with no prior anti-tumor treatment: three samples—from a 62 y.o. male undergoing total gastrectomy with confirmed diagnosis of gastric adenocarcinoma, and one sample—from a 68 y.o. male undergoing esophagogastrectomy with confirmed diagnosis of gastroesophageal junction cancer (poorly differentiated adenocarcinoma with signet ring cells).

Five samples were harvested *via* rapid autopsy (<24 h after death) from an 85 y.o. male with a confirmed lifetime diagnosis of colorectal mucinous adenocarcinoma and no prior anti-tumor treatment.

Six samples were collected *via* rapid autopsy from a 39 y.o. female with confirmed lifetime cutaneous melanoma diagnosis and history of radiation therapy and targeted therapy (dabrafenib and trametinib).

Three samples were harvested *via* rapid autopsy from an 85 y.o. female with confirmed lifetime diagnosis of breast ductal adenocarcinoma and history of radiation therapy.

Stiffness measurements

To confirm the clinical relevance of the collected *ex vivo* tumor specimens (*i.e.*, their consistency with *in vivo* studies), the Aplio i800 system (Canon, Japan) was used to measure the stiffness (Young's modulus) of six out of 18 liver metastases (secondary to gastric cancer—from two patients, and breast cancer—from one patient) and the adjacent liver parenchyma. The measurements were performed using shear wave elastography (SWE) prior to sample preparation for BH exposure (Fig. 1a). The specimens were immersed in phosphate-buffered saline (PBS) and placed on a 4-cm-high silicone absorbing layer (ToolDecor 25, BMP Technology, Russia). Young's modulus was measured at least three times per specimen using a linear 14L5 probe (Thyroid preset). Each measurement was taken within a 4-mm-diameter region of interest (ROI).

The Young's moduli were then statistically compared across different patients and between tumor and liver tissue *via* two-tailed two-sample homoscedastic Student's t-test. Significance threshold was set at $p = 0.05$.

BH study design

After the SWE measurements, all tissue specimens were dissected into smaller samples up to 4 × 3.5 × 3 cm^3 (Fig. 1b, 1c), immersed in PBS and subjected to successive cycles of degassing (three cycles of 30 min each) and compression (two cycles of 15 min each) to remove air bubbles that could potentially interfere with ultrasound propagation and interaction with tissue. After degassing, the samples were enclosed in ultrasound-transparent gel container (Fig. 1d) made of 1.5% agarose (UltraPure Agarose, Invitrogen/Thermo Fisher Scientific, Waltham, MA, USA) or 6.5% agartin (Kotanyi, Wolkersdorf im Weinviertel, Austria). The gel-embedded samples were then stored at 37°C in a laboratory thermostat heating incubator (Kasimov Instrumental Plant, Kasimov, Russia) for at least 1 hour, mounted on a 3D positioning system (Precision Acoustics UMS3, Dorchester, UK) and immersed in 35°C water (Fig. 1e) that had been degassed for 3 hours using the water treatment system (Precision Acoustics, Dorset, UK). The samples were then exposed to BH sonication through the liver capsule to imitate the clinical settings (Fig. 1b–d).

The BH focused ultrasound fields were produced using a nine-ring annular array (Fig. 1e) operating at 2-MHz frequency. The array had an 8-cm focal distance (*i.e.*, radius of curvature), 8.92-cm aperture, 4-cm diameter of the central opening, and 67.8° focusing angle. This configuration was derived from a 12-ring array described and characterized earlier [52,53], with the three outermost rings disabled. Real-time visualization for planning and monitoring the BH exposures was performed using an L7-4 diagnostic ultrasound probe (ATL, Philips, Bothell, WA, USA) aligned with the BH treatment plane (Fig. 1e) and controlled by a Verasonics V1 system (Redmond, WA, USA).

Nine out of 18 BH lesions were produced within the volume of metastases, seven lesions—at the edge of the metastases (*i.e.*, partially covering the metastasis and adjacent liver parenchyma), and two lesions were produced in liver tissue outside the metastases (Table 1). BH exposures were delivered to discrete volumetric grids (Table 1): 1–4 layers of foci transverse to the BH beam axis were sonicated sequentially from

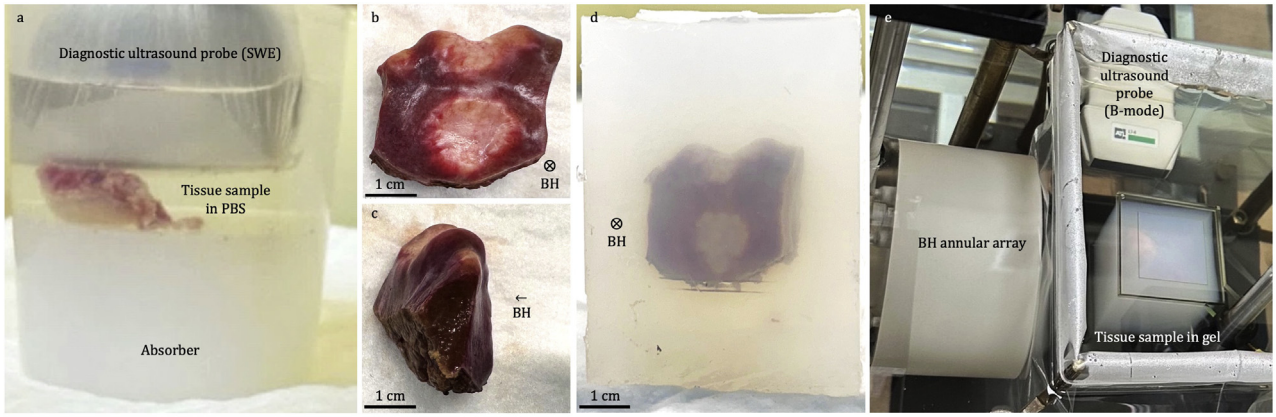

Figure 1. (a) Experimental arrangement for the Young's modulus measurements of tumor samples using shear wave elastography (SWE). (b–d) Example of sample orientation for BH exposure: before (b and c) and after (d) embedding the sample into an acoustically transparent gel. (e) Photograph of the experimental arrangement for volumetric boiling histotripsy (BH) in *ex vivo* tissue samples under B-mode diagnostic ultrasound guidance.

the deepest layer to the most superficial, to prevent emerging bubbles from interfering with ultrasound propagation and focusing. The number of sonication points in each layer varied from 3 × 3 to 5 × 5 depending on the sample size to fit the target volume within the sample while preserving part of the surrounding tumor for evaluation of the damage margins. The spacing between sonication points was 1 mm in all directions. The pulse duration was kept at 1 ms with 1% duty cycle (*i.e.*, a pulse repetition frequency of 10 Hz), while the number of pulses per point (hereinafter referred to as *ppp*) varied from 25 to 200 ppp. Prior to volumetric BH exposure in each sample, the threshold value of the BH pulse output voltage was determined experimentally by incrementally increasing the voltage of isolated 1-ms pulses. These pulses were delivered to the corner points of the planned lesion until vapor bubbles appeared within the BH focal region, manifested as a hyperechoic zone on B-mode imaging. For volumetric BH exposure, the voltage was set 43%–50% above the threshold to ensure effective disintegration of the target volume, accounting for potential acoustic inhomogeneities along the BH beam path. The corresponding peak acoustic power within the pulse varied from 65 to 270 W, depending on the depth and location of the target volume. The average depth of the focus in tissue was 7.4 mm. The corresponding pressure estimations at the transducer surface and *in situ* are detailed in the next section.

Numerical modeling of the BH fields in situ

Acoustic characterization of the BH annular array in water was performed earlier in [52,53] by low-amplitude hydrophone measurements and high-amplitude numerical modeling to characterize the linear and nonlinear ultrasound fields, respectively. Here, the high-amplitude fields were modeled in the tissue samples using the "HIFU beam" software [54] for a flat-layered medium consisting of water (35°C) followed by liver tissue (Fig. 2a). The nominal geometric parameters of the array were used for setting a boundary condition (Fig. 2b). Characteristic pressure amplitude at the array surface ranged from 0.2 to 0.415 MPa, corresponding to an acoustic power range of 65–270 W. These values were established in previous studies based on a combination of the acoustic holography measurements and nonlinear simulations at increased power outputs [52,53,55]. The acoustic parameters of liver were taken from [56,57] and were as follows: speed of sound $c = 1586$ m/s, density $\rho = 1079$ kg/m^3, non-linearity coefficient $\beta = 4.64$, diffusivity coefficient $\delta = 4.33$ mm^2/s, and absorption coefficient $\alpha = 0.1383$ Np/cm at 2 MHz frequency, with a power law of absorption $\nu = 1.1$.

Simulation results obtained for the average focal depth in tissue across all samples (7.4 mm) and the mean acoustic power across all exposures (175 W) are shown in Figure 2 (c–f). The focal pressure waveform,

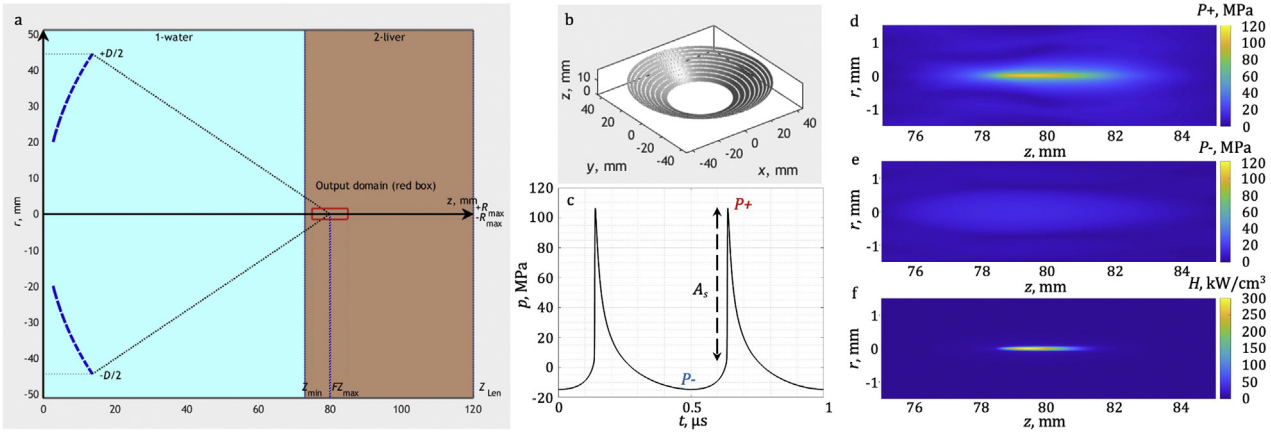

Figure 2. Numerical modeling of focused ultrasound fields in tissue samples using "HIFU beam" software. (a) Schematics of the numerical experiment. (b) 3D model of the BH array geometry. (c–f) *In situ* field parameters simulated at the average power and focal depth in tissue: (c) two cycles of acoustic pressure waveform at the axial peak pressure point, (d–f) 2D distributions of the peak positive $P+$ (d) and peak negative $P-$ (e) pressures, and heat deposition rate H (f) in the axial plane around the geometric focus of the array ($z = 80$ mm).

presented in Figure 2c, exhibits a distinct asymmetric profile for each cycle. It is characterized by a high peak positive pressure ($P+ = 106.4$ MPa), a much lower peak negative pressure ($P- = -14.8$ MPa), and a high-amplitude shock front ($A_s = 101.1$ MPa). The spatial distributions of acoustic field parameters in tissue shown in Figure 2 (d, e) differ significantly for the peak positive and negative pressures. The axial and lateral dimensions of the focal region at −6 dB level are 3.33 mm × 0.24 mm for the peak positive pressure, which is considerably smaller than the dimensions of 7.65 mm × 1.18 mm for the peak negative pressure. The heat deposition rate is primarily determined by the strong absorption of acoustic energy at the shock fronts. This process is concentrated within a very small region of 1.78 mm × 0.1 mm (defined at the half-maximum level) where the peak value reaches $H = 293$ kW/cm^3. The time to reach boiling in tissue at the focus was estimated from this maximum value H of energy absorption as $t_b = \frac{\Delta T c_v}{H}$ [28], where $c_v = 3.82$ MJ/(m^3 K) [56] is the heat capacity per unit volume of liver tissue, ΔT is the temperature difference between the initial tissue temperature (35°C as in the surrounding water) and the boiling point (100°C), and H is the maximum heat deposition rate *in situ* obtained in simulations. The resulting estimated time-to-boil was $t_b = 0.85$ ms, which is consistent with experimental observations of tissue boiling occurring within each 1-ms BH pulse.

Post-treatment evaluation of tissue microstructure

Following BH exposure and B-mode imaging of the resulting lesions, samples were extracted from the gel containers. The treatment and imaging plane orientations were marked on the sample surface with histological ink (HistoSafe, Russia), and the samples were fixed in 10% neutral buffered formalin (Labiko, Russia) for 4 weeks. Subsequently, the tissue was dissected into 2-mm thick blocks along the imaging plane, processed, embedded in paraffin wax, sectioned into 1−3-μm thick sections, and mounted on microscopic slides. The slides were then stained with hematoxylin-eosin (H&E, standard histological stain) and Masson's trichrome (MT, three-color stain for differentiation of collagen fibers that stain blue or green) and digitalized using a Leica SCN 400 slide scanner (component of Interactive microscope system, 441-2010, ID 9351706). Histological evaluation of the resulting slides and estimation of lesion volumes and corresponding treatment rates were performed by a certified clinical pathologist (initials N.D.). It should be noted that tissue specimens tend to shrink during formalin fixation [58], leading to underestimation of lesion volumes and, consequently, treatment rates.

Liquefied tumor mass from one volumetric BH lesion was collected with a scalpel. The lysate was either mounted on a carbon double-sided tape for scanning electron microscopy (SEM) or suspended in distilled water to isolate residual fragments and placed on a glass substrate for transmission electron microscopy (TEM). All samples were then fixed in 2.5% glutaraldehyde solution and processed for SEM and TEM as previously described [59]. SEM samples were imaged using a JEOL JSM-6380LA Analytical Scanning Electron Microscope (Tokyo, Japan), while TEM samples were imaged using a JEOL JEM-1011 Transmission Electron Microscope (Tokyo, Japan).

Results

Clinical relevance of ex vivo *tissue stiffness*

To confirm that the *ex vivo* tumor specimens were clinically relevant and consistent with *in vivo* conditions, the sample stiffness (Young's modulus) was measured in liver metastases secondary to gastric and breast cancer. The SWE-measured stiffness values fell within the clinically observed range [60]—from 21.6 to 79.6 kPa (median: 44 kPa)—regardless of tumor origin: 23 ± 1 kPa and 49.4 ± 6.8 kPa in tumors secondary to gastric cancer (41.3 ± 14.1 kPa if averaged across two patients) and 48.7 ± 21.6 kPa in tumors secondary to breast cancer. *Ex vivo* liver metastases were clearly distinguishable on both B-mode images and Young's modulus color maps. Regardless of tumor origin, the metastases were significantly stiffer than the adjacent liver parenchyma (Fig. 3): 44 ± 17 kPa vs. 9.3 ± 3.9 kPa ($p < 9 \times 10^{-5}$).

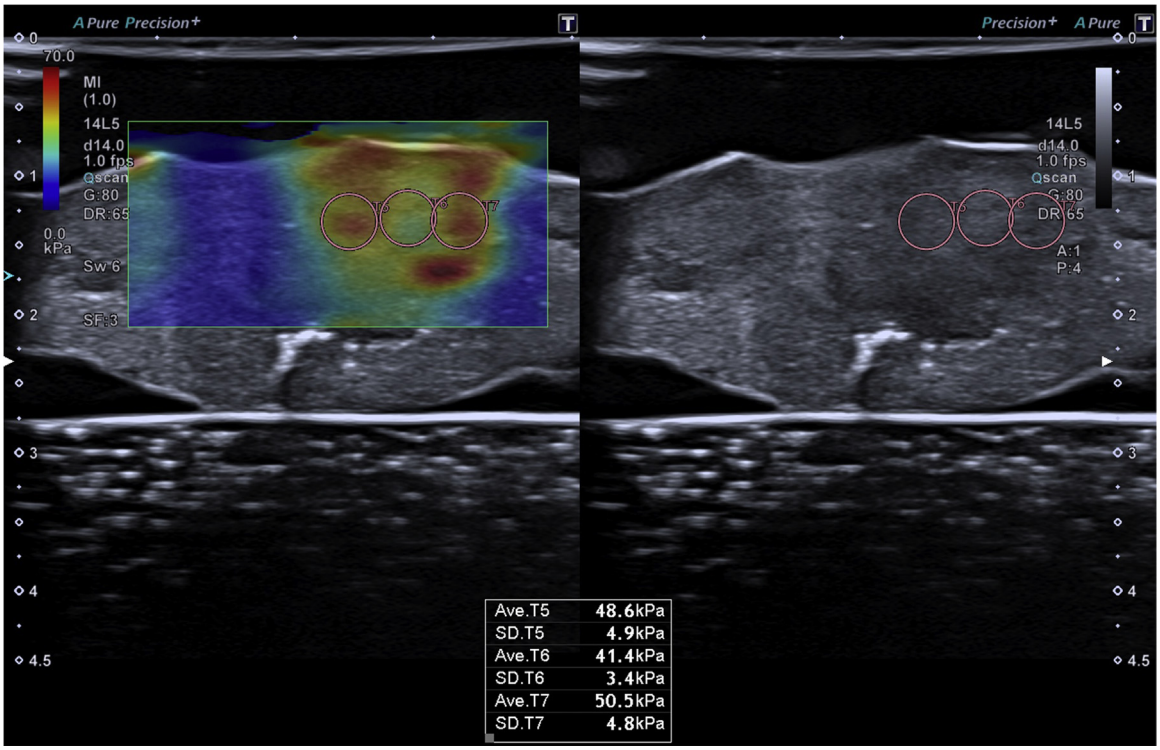

Figure 3. Representative image of the shear wave elastography measurements of Young's moduli of liver metastasis secondary to gastric cancer: (*left*) Young's modulus color map, (*right*) the corresponding B-mode image. In this example, three regions of interest (ROIs), indicated by red circles, were sampled within the metastasis. The resulting average values of the Young's moduli and standard deviations are summarized in the table at the *bottom* of the image.

Gastric cancer liver metastases with no prior treatment

Liver metastases secondary to gastric cancer exhibited echogenicity on B-mode imaging similar to the surrounding liver tissue; however, the tumor boundaries could be visually distinguished (Figs. 3 and 4a).

Figure 4 shows two BH lesions produced in one of the gastric cancer metastases at 75 ppp (upper lesion) and 150 ppp (lower lesion). During and immediately after the BH exposure, the target volume appeared hyperechoic on B-mode, a typical observation for BH that indicates the presence of bubbles in the target area (Fig. 4b, 4c). The treated volumes became hypoechoic within 10 min post-treatment (Fig. 4d) as bubbles dissolved, leaving the liquefied tissue without scatterers. This characteristic BH response corresponded well in shape and size with the lesions observed after bisection of the formalin-fixed samples along the B-mode imaging plane (Fig. 4e). Further histological analysis of the sample microstructure revealed that both exposure protocols (with 75 and 150 ppp) produced sharply demarcated, homogeneous lesions with indiscernible cellular structure throughout the predominant portion of the lesion volume (Fig. 4f–j). Reducing the pulse number from 150 to 75 pulses per point (ppp) led to an increase in the maximum size of residual tissue fragments from 100 to 300 μm. However, the estimated volumetric treatment rate increased by 89%—from 28.4 to 53.6 mm^3/min—because the treatment time was halved (from 8 to 4 min) while the lesion volume decreased only modestly from 227.3 to 214.2 mm^3. Figure 4g also demonstrates higher resistance of vascular structures to mechanical disintegration than that of the tumor tissue or liver parenchyma, which was typical for BH [61]: the distal part of the lesion is confined by the portal tract whereas the lesion in Figure 4h extends beyond the tumor volume into the liver parenchyma.

Further reduction in the number of pulses to 50 ppp also resulted in the formation of a homogeneously liquefied lesion (Fig. 5). Despite producing the smallest lesion volume (101 mm^3) compared to the exposures with 75 and 150 ppp, this setting provided a higher treatment rate (37.8 mm^3/min) than the 150 ppp protocol.

These surgically-resected gastric cancer metastases in liver had not been subjected to any prior anti-tumor therapy; however, histological examination revealed signs of extensive spontaneous coagulative necrosis of the tumors. This finding is characteristic for metastatic liver disease [62] and was clearly distinguishable from the adjacent BH-induced tissue disintegration with completely undiscernible cellular structure (Fig. 5c, 5d).

Colorectal cancer liver metastases with no prior treatment

In liver metastases secondary to colorectal mucinous adenocarcinoma, both 50 and 25 ppp were sufficient for mechanical disintegration of tumor cells, fibrous septa dividing the extracellular mucin lakes, and

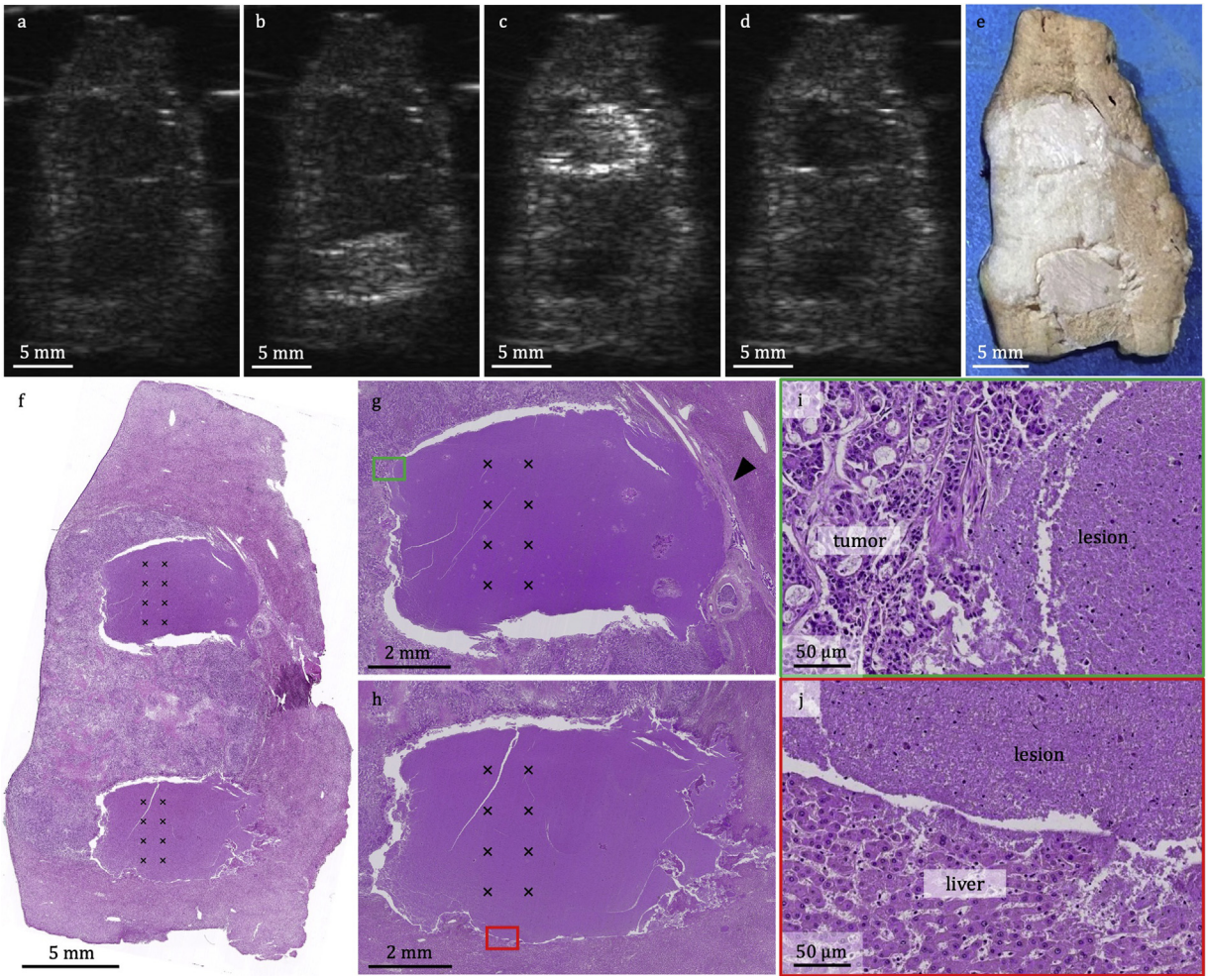

Figure 4. Illustration of the two volumetric BH lesions produced in gastric cancer metastasis in liver (with spontaneous necrosis and no prior anti-tumor therapy) with 75 (*upper lesion*) and 150 (*lower lesion*) pulses per sonication point. (a–d) B-mode images of the sample: (a) before BH exposure, (b and c) immediately after generation of the *lower* (b) and *upper* (c) lesions, (d) 10 min after generation of the upper lesion and 50 min after generation of the lower lesion. (e) The same sample after formalin fixation and bisection along the B-mode imaging plane. (f–j) H&E-stained histological images of the produced lesions: (f) whole-mount section of the sample, (g and h) magnified zones containing the lesions, (i and j) lesion borders with tumor (i) and liver parenchyma (j) at higher magnification. Arrowhead in (g) points at the portal tract confining the lesion post-focally. BH exposure incident from the *left* in all images. ×-symbols indicate the approximate positions of the sonicated points.

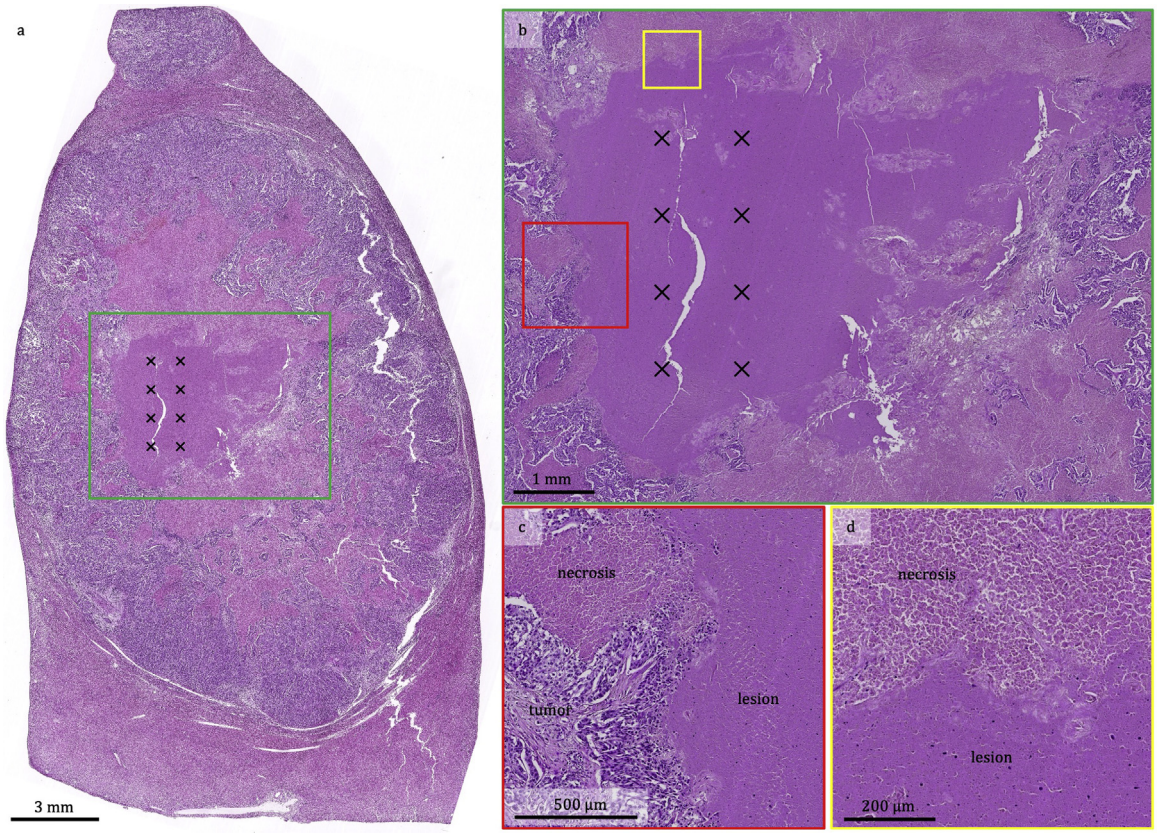

Figure 5. H&E-stained histological images of a volumetric BH lesion produced in gastric cancer metastasis in liver (with spontaneous necrosis and no prior anti-tumor therapy) at 50 pulses per sonication point: (a) whole-mount section of the sample, (b) magnified zone containing the lesion, (c and d) lesion borders at higher magnifications. Frame (d) illustrates the difference in microstructure of spontaneously necrotized tissue and BH-induced disintegration. BH exposure incident from the left in all images. ×-symbols indicate the approximate positions of the sonicated points.

liver parenchyma within the target volume (Fig. 6). The use of a lower number of pulses (25 vs. 50 ppp), however, resulted in less homogeneous fragmentation, larger residual tissue fragments within the lesion, smaller lesion volume (120 vs. 142 mm^3), yet higher treatment rate (38.3 vs. 22.7 mm^3/min). Although these autopsy samples were collected from the patient with no history of anti-tumor treatment, the colorectal cancer metastases showed regions of spontaneous coagulative necrosis in liver (Fig. 6a, 6d) which may be associated with postmortem changes or spontaneous necrosis common in large rapidly growing tumors.

While no difference in response to BH treatment was observed between the liver parenchyma and metastases secondary to gastric adenocarcinoma or melanoma, some histological sections suggested possible greater resistance of colorectal mucinous adenocarcinoma to BH compared with adjacent liver tissue: one side of the BH lesions was confined by post-focally located metastases (indicated by the two arrows in Fig. 6a, 6d, 6g, 6j) while the other side extended further into the liver parenchyma (indicated by the single arrow in Fig. 6a, 6d, 6g, 6j).

Melanoma liver metastases with prior targeted and radiation therapy

Autopsy-derived liver metastases secondary to melanoma appeared hypoechoic relative to the adjacent liver parenchyma on B-mode ultrasound (Fig. 7a). Histological examination revealed hemorrhage and partial necrosis outside the BH-treated zone (Fig. 7c–d), likely resulting from prior targeted and radiation therapy. All melanoma metastases were successfully disrupted with 150-ppp BH protocol, confirming treatment reproducibility. This resulted in hypoechoic volumes on post-treatment B-mode imaging (Fig. 7b) and homogeneously acellular zones with sharply demarcated boundaries (<100 μm in width) on histological examination (Fig. 7e–g). The average BH treatment rate in melanoma metastases was 13.3 ± 6.6 mm^3/min (from 7.6 to 24.5 mm^3/min depending on the sonication geometry).

Breast cancer liver metastases with prior radiation therapy

Extensive tumor fibrosis was observed in ductal carcinoma metastases in liver, likely as a consequence of prior radiation therapy (Fig. 8), which increased tumor resistance to BH treatment. BH exposures at 100 and 150 ppp that were effective in non-fibrotic metastases were insufficient for complete liquefaction of the target volume of fibrotic tumor mass, selectively fragmenting non-fibrotic tumor components while only partially disrupting the collagen stroma (Fig. 8, left and center columns). The use of 200 ppp was required to disintegrate both cellular and fibrotic tumor components within the target volume (Fig. 8, right column) leaving individual undertreated, yet non-viable collagen fragments within the treated zone (Fig. 8f, 8l). The treatment rate for such successful exposure in collagen-rich breast carcinoma was 14.2 mm^3/min.

Electron microscopy of the liquefied tumor suspension

Figure 9 illustrates the ultrastructure of the content collected from the treated volume and examined using scanning and transmission electron microscopy (SEM and TEM). Similar to other tissues exposed to BH [30,59,63], SEM imaging of undiluted lesion content showed multi-layered structureless cellular debris (Fig. 9a). TEM imaging of the material suspended in distilled water allowed for distinguishing separate damaged collagen fibers, fragmented cells, and cell components (Fig. 9b–f), thus confirming the ability of BH to mechanically disintegrate liver metastases into subcellular debris.

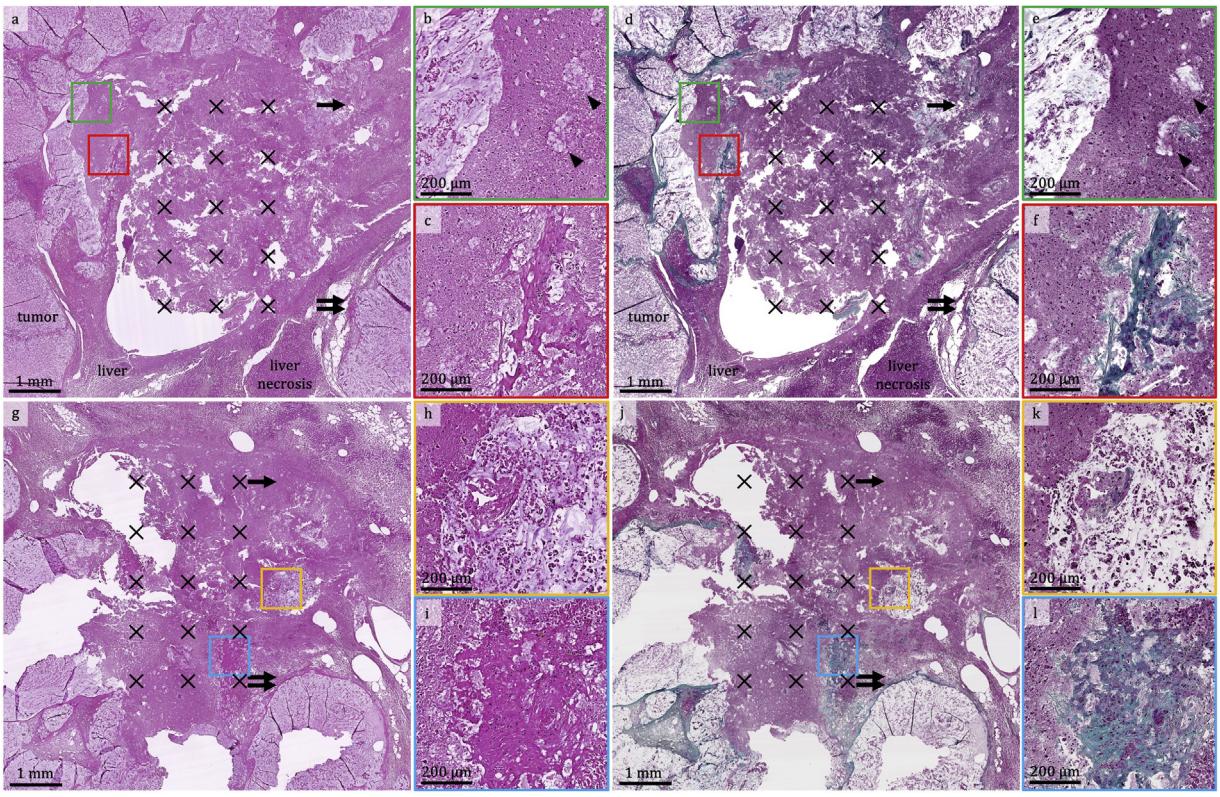

Figure 6. Histological images of the two volumetric BH lesions produced in colorectal cancer metastasis in liver (with spontaneous necrosis in liver and no prior anti-tumor therapy) at 50 (a–f) and 25 (g–l) pulses per sonication point, stained with H&E (a–c, g–i) and Masson's trichrome (d–f, j–l). (a, d, g, j) Magnified zones containing the lesions, (b and e) border between lesion and tumor at higher magnification, (h,k) residual tumor fragments within the lesion volume, (c, f, i, l) residual damaged collagen fibers within the lesion volume. The *single arrow* points at disrupted liver parenchyma in the distal part of the lesion, the two *arrows* point at intact metastases in distal part of the lesion. *Arrowheads* point at disrupted fragments of mucin within the lesion. BH exposure incident from the *left* in all images. ×-symbols indicate the approximate positions of the sonicated points.

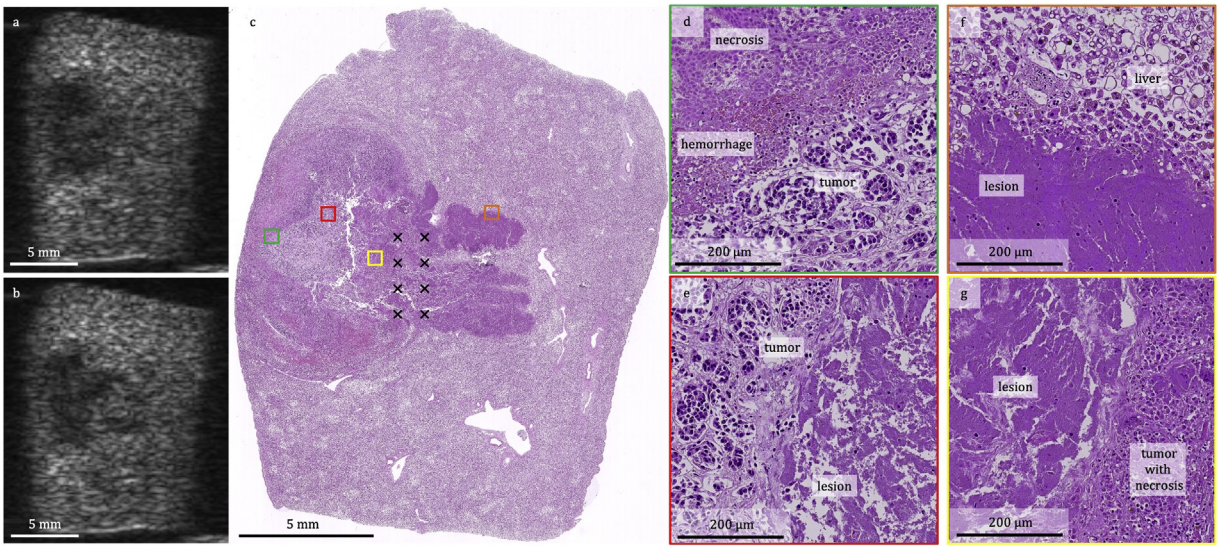

Figure 7. Volumetric BH lesion produced in melanoma metastasis in liver (with necrosis and prior targeted and radiation therapy) at 150 pulses per sonication point. (a and b) B-mode images of the sample: pre-treatment (a) and 10 min after the BH treatment (b). (c–g) H&E-stained histological images of the produced lesion: (c) whole-mount section of the sample, (d) magnified zone outside the lesion containing intact tumor, hemorrhage and tumor necrosis, (e and f) lesion borders with tumor (e) and fatty liver parenchyma (f) at higher magnification, (g) magnified zone containing undertreated tumor tissue inside the lesion. BH exposure incident from the *left* in all images. ×-symbols indicate the approximate positions of the sonicated points.

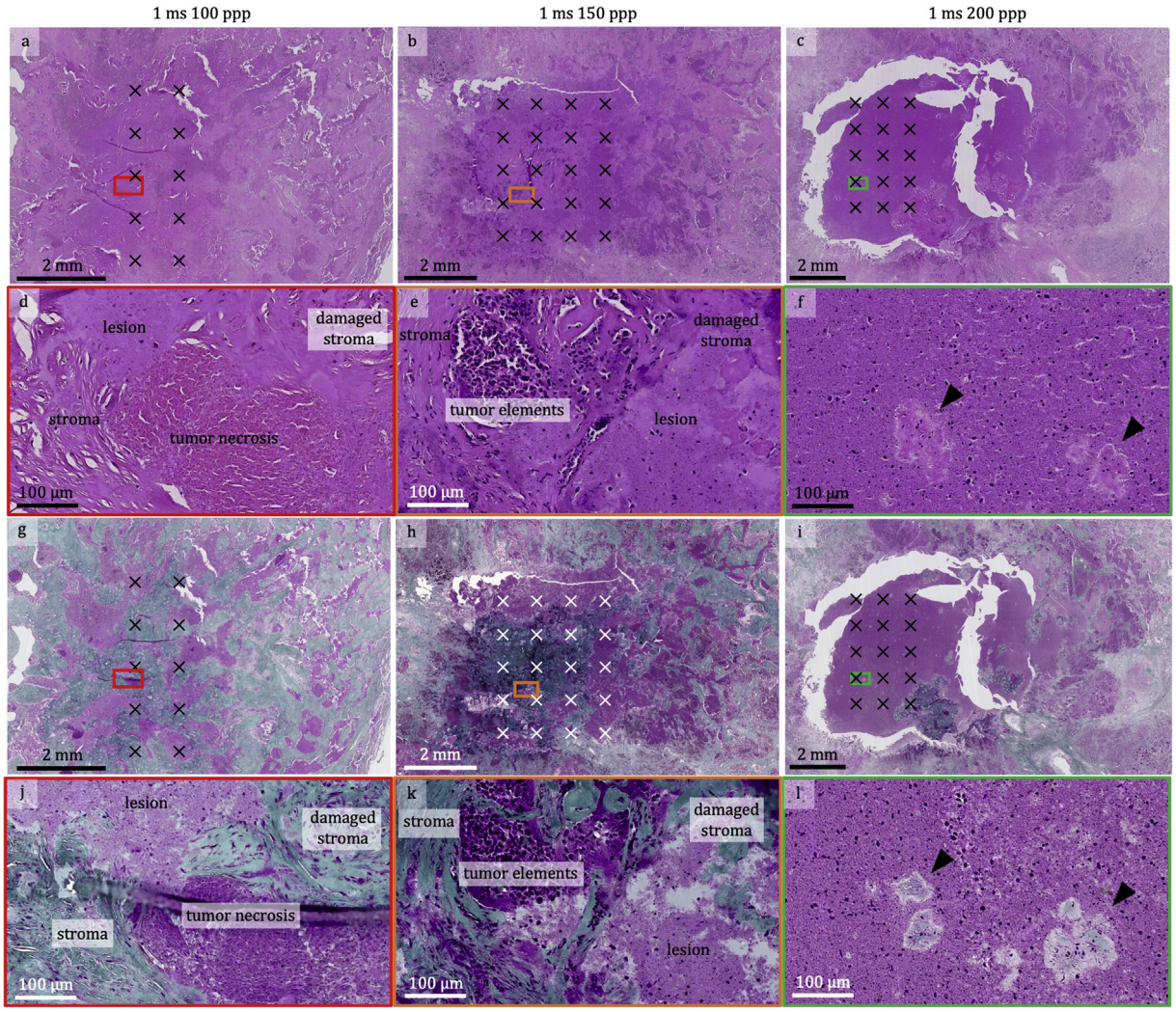

Figure 8. Histological images of the three volumetric BH lesions produced in breast cancer metastasis in liver (with radiation-induced fibrosis) with 100 (*left column*), 150 (*central column*) and 200 (*right column*) pulses per sonication point stained with H&E (a–f) and Masson's trichrome (g–l). (a–c and g–i) Magnified zones containing the lesions, (d–f and j–l) magnified zones within the lesions. *Arrowheads* point at remained fragments of damaged collagen. BH exposure incident from the *left* in all images. ×-symbols indicate the approximate positions of the sonicated points.

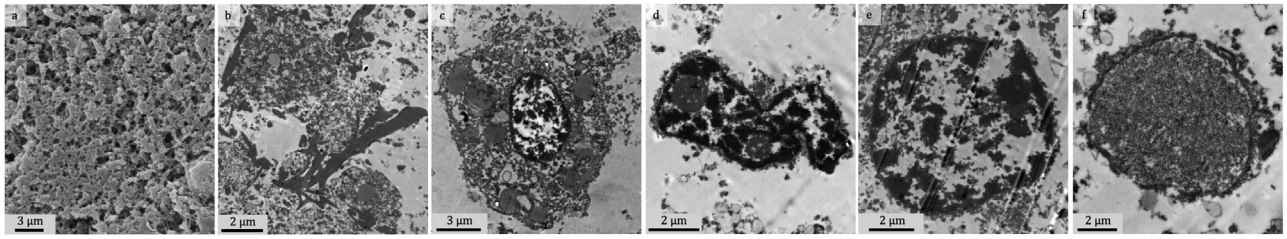

Figure 9. Representative electron microscopy images of the liquefied content of gastric cancer metastasis in liver. (a) Scanning electron microscopy image showing multi-layered fragments of fractionated tissue, (b–f) transmission electron microscopy images of diluted lesion content: (b) cellular debris and fragments of damaged collagen fibers, (c) damaged cell with intact nucleus surrounded by fragmented cellular components and lysosomes, (d) cell nucleus with damaged membrane and two nucleoli inside, (e) cell nucleus with damaged membrane, (f) probably damaged mitochondria.

Discussion

This study provides the first *ex vivo* demonstration that BH can mechanically disintegrate planned volumes in human liver metastases of various origins and history of anti-tumor treatment. Our findings indicate that liver tumors secondary to gastric, colorectal, breast, and skin (melanoma) cancers can be non-invasively fragmented into subcellular debris using a sequence of 1-ms focused ultrasound pulses with shock fronts under diagnostic ultrasound guidance. The most significant finding is that the required number of BH pulses is highly dependent on the microstructure of the tumor, particularly the presence of necrosis or fibrosis, which has direct implications for clinical treatment planning.

Our data suggest that a personalized approach to BH treatment planning is not only feasible but necessary. Metastases with prior therapy-induced necrosis or spontaneous necrosis, common in large, rapidly growing liver masses [62], can be effectively disintegrated with fewer

pulses per sonication point than fibrotic metastases. These fibrotic changes, typical after radiation therapy [64], should be accounted for during pre-treatment planning step. In particular, the lowest number of pulses per point successfully employed in this study for the treatment of tumors containing necrotic zones was 25 ppp, while tumors with radiation-induced fibrosis required at least 200 ppp for complete disintegration of both cellular and collagen-rich components within the target volume. Consequently, when planning the complete volumetric treatment of a fibrotic metastasis, a higher number of pulses or longer pulse durations (*e.g.*, 5–10 ms) should be considered. The use of longer pulses has been shown to be more effective for mechanical ablation of collagen-rich tissues [39]. Pre-treatment assessment using shear wave elastography or contrast-enhanced CT or MRI could identify necrotic or fibrotic tumor regions [51], enabling the development of a patient-specific spatially modulated BH dosing plan with higher doses (*i.e.*, greater number of pulses per point or longer pulses) delivered to fibrotic and lower doses to necrotic regions.

An intriguing finding is that the use of intermediate number of BH pulses (100–150 ppp) in fibrotic tumors led to selective fragmentation of cellular components while preserving parts of the collagen stroma. This selective damage may be sufficient to eradicate viable tumor cells while potentially preserving the extracellular matrix. Moreover, even weaker damage with partial disruption of cancer cells may be beneficial for destabilizing the tumor microenvironment. In the context of histotripsy-induced immunomodulation and abscopal effect, such damage may release tumor antigens while simultaneously inducing immunogenic cell death, thereby potentially stimulating a systemic anti-tumor immune response [45–48]. This is particularly relevant for malignancies such as melanoma, which are highly responsive to immunotherapy [49,65]. Thus, BH could be employed not only for complete tumor disintegration but also for partial tumor disruption. Such an approach could potentially serve as an *in situ* vaccination tool in combination with immune checkpoint inhibitors, a strategy actively being explored for histotripsy [50,66–68], and other ablation modalities [69,70]. Alternatively, our findings also suggest that BH may be used not only as a standalone procedure or neoadjuvant strategy to reduce tumor mass and minimize the extent of subsequent surgical resection, but also as a tool following prior anti-tumor therapy to ensure complete removal of residual, non-responsive parts of the tumor.

Another clinically important feature of BH demonstrated in both previous studies [61] and the present work is its ability to spare critical vascular structures while effectively fragmenting the adjacent parenchyma. In addition, unlike thermal techniques such as HIFU or RFA, the mechanical action of BH is not subject to the heat-sink effect. Together, these features make BH a potentially viable treatment option for patients with liver masses in immediate proximity to major vessels who are otherwise ineligible for minimally invasive ablation strategies [12–14].

Histologically, the majority of the liver tumors that were demonstrated here to susceptible to BH were adenocarcinomas, which is the most common subtype of liver metastases, followed by melanoma [71], which was also investigated in this work. Moreover, the primary sites of the studied liver tumors were among the most frequent origins of liver metastases, thus confirming the clinical relevance of the liver tumors treated with BH in this study. Primary liver tumors can also be assumed to be amenable to BH treatment, given the structural similarities they share with adenocarcinomas investigated here.

A systemic comparative analysis of the response to BH between tumor tissue and surrounding liver parenchyma was beyond the scope of this study, however, our preliminary findings here indicated similar susceptibility to BH of liver parenchyma and liver tumors secondary to melanoma and gastric adenocarcinoma. Some of the obtained results, however, suggested that mucinous adenocarcinoma secondary to colorectal cancer may exhibit greater resistance to BH than the adjacent liver parenchyma, likely due to the presence of fibrous septa surrounding and separating the densely packed extracellular mucin lakes. Although further comparative studies are required, the potentially lower resistance of liver parenchyma to BH may be advantageous clinically, as it could enhance procedural safety by facilitating disintegration of the hepatic margin surrounding the treated tumor, typically resected surgically along with the tumor mass.

The treatment rates obtained in this pilot study for complete disintegration of the planned tumor volumes, estimated from formalin-fixed (and therefore slightly shrunken) samples, was up to 53.6 mm^3/min, which is below values reported in clinical practice for thermal HIFU ablation of liver tumors (around 0.33 cm^3/min, indirectly estimated from [72]) and in the ongoing clinical trial for cavitation-based histotripsy (around 0.5 cm^3/min, indirectly estimated based on MRI from [24]). However, the primary objective of this pilot study was not to maximize treatment speed but to establish fundamental feasibility and dose–response relationships. Our findings identify clear pathways toward optimizing BH parameters to achieve clinically competitive treatment rates. These include increasing the spacing between sonication points (based on the focal zone dimensions and the sizes and quality of the produced volumetric BH lesions), using longer pulses to generate larger lesions [73], and tailoring the number of pulses per point based on tumor microstructure. Moreover, for immunomodulation purposes or disruption of tumor microenvironment, where complete disintegration may not be necessary, lower doses and larger spacing could be used, further accelerating the procedure.

While SWE measurements confirmed clinical relevance of the Young's moduli of these *ex vivo* liver metastases and agreed with literature regarding higher tumor stiffness *vs* the surrounding liver parenchyma [60], the transition from a controlled *ex vivo* environment to clinical practice involves several challenges. Within a clinical context, the transcutaneous focusing of the BH beam on targets in the liver may induce substantial acoustic aberrations and attenuation arising from propagation through structurally and acoustically heterogeneous tissues. This contrasts with the present pilot investigation, in which BH treatment was performed under controlled laboratory conditions in a water tank using *ex vivo* tissue specimens. However, the use of multi-element BH arrays allows for adaptive real-time aberration correction through element phasing, which has been successfully demonstrated in animal models *in vivo* [40,74]. Moreover, the operating output voltage in the present study was set well above the experimentally determined threshold value (by 43%–50%), whereas BH has been shown to be feasible *in vivo* at voltage values only 10% above the threshold [40]. This suggests the potential to compensate for ultrasound energy attenuation caused by intervening tissues *in vivo*, thereby ensuring the formation of shock fronts sufficient to enable BH at the focus.

Another challenge inherent to *in vivo* settings, compared with the present *ex vivo* study, is the significant motion and deformation of the liver with respiration. However, our recent *in vivo* study in porcine liver demonstrated that tracking the skin surface above the liver using conventional diagnostic ultrasound allows BH delivery to be gated to the respiratory cycle. By suspending pulses during the inhalation phase, off-target tissue damage can be prevented without requiring complex motion compensation strategies [40].

In clinical transcutaneous implementation of BH for liver tumors, some targets may be obstructed by the ribs, bowel gas, or lung segments. Such obstacles can attenuate or distort the beam, hindering the precise focusing and shock-front formation required for BH [18,75–78]. However, the lower pressure requirements of BH relative to CH allow for the use of transducers with a smaller footprint [30,59,63,79–81]. This compact design potentially expands the treatment window and enables laparoscopic or intraoperative access, offering a hybrid minimally invasive solution for anatomically challenging malignancies.

Conclusion

This *ex vivo* study is the first to demonstrate the potential of BH to mechanically disintegrate defined volumes within human liver metastases of various origins using focused millisecond-long ultrasound pulses

with shock fronts under diagnostic ultrasound guidance. Such treatment can potentially be used both as a standalone procedure and as a neoadjuvant tool, or following prior anti-tumor therapy. BH treatment can be accelerated by reducing the number of pulses for non-fibrotic or necrotic tumors, while fibrosis induced by prior anti-tumor treatment complicates treatment and necessitates a higher number of BH pulses for complete tumor disintegration.

Conflict of interest

The authors declare no competing interests.

Data availability statement

Data will be made available on request.

Acknowledgments

This work was supported by the Russian Science Foundation [grant 25-12-00157]. Leica SCN 400 slide scanner acquired under the MSU development program was used for digitalization of the histological slides. The authors thank S.A. Usmanova for preparing histological specimens and A.G. Bogdanov from the Electron Microscopy Laboratory of the Biological Faculty of the MSU for help with SEM and TEM analysis.

References

[1] Griscom JT, Wolf PS. Liver metastasis. StatPearls. Treasure Island (FL): StatPearls Publishing; 2023.
[2] Benson AB, Venook AP, Adam M, Chang G, Chen YJ, Ciombor K, et al. NCCN guidelines® insights: rectal cancer, version 3.2024. J Natl Compr Canc Netw 2024;22(6):366–75. doi: 10.6004/jnccn.2024.004.
[3] Bray F, Laversanne M, Sung H, Ferlay J, Siegel RL, Soerjomataram I, Jemal A. Global cancer statistics 2022: GLOBOCAN estimates of incidence and mortality worldwide for 36 cancers in 185 countries. CA Cancer J Clin 2024;74(3):229–63. doi: 10.3322/caac.21834.
[4] Horn SR, Stoltzfus KC, Lehrer EJ, Dawson LA, Tchelebi L, Gusani NJ, et al. Epidemiology of liver metastases. Cancer Epidemiol 2020;67:101760. doi: 10.1016/j.canep.2020.101760.
[5] Weiss L. Comments on hematogenous metastatic patterns in humans as revealed by autopsy. Clin Exp Metastasis 1992;10(3):191–9. doi: 10.1007/BF00132751.
[6] Wang Q. Targeted therapy for liver cancer: current status and future directions. Bioimpacts 2025;15:32630. doi: 10.34172/bi.32630.
[7] Deng GL, Zeng S, Shen H. Chemotherapy and target therapy for hepatocellular carcinoma: new advances and challenges. World J Hepatol 2015;7(5):787–98. doi: 10.4254/wjh.v7.i5.787.
[8] Wu D, Jia B, Jia M, Zhao H, Zhao H, Zhou J. Comparative efficacy and safety of systemic therapy for advanced hepatocellular carcinoma: a systematic review and network meta-analysis. Front Oncol 2023;13:1274754. doi: 10.3389/fonc.2023.1274754.
[9] Zheng J, Wang S, Xia L, Sun Z, Chan KM, Bernards R, et al. Hepatocellular carcinoma: signaling pathways and therapeutic advances. Signal Transduct Target Ther 2025;10(1):35. doi: 10.1038/s41392-024-02075-w.
[10] Kroese TE, van Laarhoven HWM, Nilsson M, Lordick F, Guckenberger M, Ruurda JP, et al. Definition of oligometastatic esophagogastric cancer and impact of local oligometastasis-directed treatment: a systematic review and meta-analysis. Eur J Cancer 2022;166:254–69. doi: 10.1016/j.ejca.2022.02.018.
[11] Adnan A, Sheth RA, Tam A. Oligometastatic disease in the liver: the role of interventional oncology. Br J Radiol 2022;95(1138):20211350. doi: 10.1259/bjr.20211350.
[12] Abdalla M, Collings AT, Dirks R, Onkendi E, Nelson D, Ozair A, et al. Surgical approach to microwave and radiofrequency liver ablation for hepatocellular carcinoma and colorectal liver metastases less than 5 cm: a systematic review and meta-analysis. Surg Endosc 2023;37(5):3340–53. doi: 10.1007/s00464-022-09815-5.
[13] Hui TC, Kwan J, Pua U. Advanced techniques in the percutaneous ablation of liver tumours. Diagnostics (Basel) 2021;11(4):585. doi: 10.3390/diagnostics11040585.
[14] Cheung TT, Ma KW, She WH. A review on radiofrequency, microwave and high-intensity focused ultrasound ablations for hepatocellular carcinoma with cirrhosis. Hepatobiliary Surg Nutr 2021;10(2):193–209. doi: 10.21037/hbsn.2020.03.11.
[15] Kennedy JE, Wu F, ter Haar GR, Gleeson FV, Phillips RR, Middleton MR, et al. High-intensity focused ultrasound for the treatment of liver tumours. Ultrasonics 2004;42(1-9):931–5. doi: 10.1016/j.ultras.2004.01.089.
[16] Hsiao YH, Kuo SJ, Tsai HD, Chou MC, Yeh GP. Clinical application of high-intensity focused ultrasound in cancer therapy. J Cancer 2016;7(3):225–31. doi: 10.7150/jca.13906.
[17] Ji Y, Zhu J, Zhu L, Zhu Y, Zhao H. High-intensity focused ultrasound ablation for unresectable primary and metastatic liver cancer: real-world research in a Chinese tertiary center with 275 cases. Front Oncol 2020;10:519164. doi: 10.3389/fonc.2020.519164.
[18] Sehmbi AS, Froghi S, Oliveira de Andrade M, et al. Systematic review of the role of high intensity focused ultrasound (HIFU) in treating malignant lesions of the hepatobiliary system. HPB (Oxford) 2021;23(2):187–96. doi: 10.1016/j.hpb.2020.06.013.
[19] Yu T, Luo J. Adverse events of extracorporeal ultrasound-guided high intensity focused ultrasound therapy. PLoS One 2011;6(12):e26110. doi: 10.1371/journal.pone.0026110.
[20] Xu Z, Hall TL, Vlaisavljevich E, Lee Jr. FT. Histotripsy: the first noninvasive, non-ionizing, non-thermal ablation technique based on ultrasound. Int J Hyperthermia 2021;38(1):561–75. doi: 10.1080/02656736.2021.1905189.
[21] Williams RP, Simon JC, Khokhlova VA, Sapozhnikov OA, Khokhlova TD. The histotripsy spectrum: differences and similarities in techniques and instrumentation. Int J Hyperthermia 2023;40(1):2233720. doi: 10.1080/02656736.2023.2233720.
[22] Queen H, Ferris SF, Cho CS, Ganguly A. The emerging role of histotripsy in liver cancer treatment: a scoping review. Cancers (Basel) 2025;17(6):915. doi: 10.3390/cancers17060915.
[23] Parsons JE, Cain CA, Abrams GD, Fowlkes JB. Pulsed cavitational ultrasound therapy for controlled tissue homogenization. Ultrasound Med Biol 2006;32(1):115–29. doi: 10.1016/j.ultrasmedbio.2005.09.005.
[24] Mendiratta-Lala M, Wiggermann P, Pech M, Serres-Créixams X, White SB, Davis C, et al. The #HOPE4LIVER single-arm pivotal trial for histotripsy of primary and metastatic liver tumors. Radiology 2024;312(3):e233051. doi: 10.1148/radiol.233051.
[25] Wehrle CJ, Burns K, Ong E, Couillard A, Parikh ND, Caoili E, et al. The first international experience with histotripsy: a safety analysis of 230 cases. J Gastrointest Surg 2025;29(4):102000. doi: 10.1016/j.gassur.2025.102000.
[26] Uysal M, Wehrle CJ, Satish S, Knott E, Hong H, Allkushi E, et al. Histotripsy of liver tumors: patient selection, ethical discussions, and how we do it. Cancers (Basel) 2025;17(7):1100. doi: 10.3390/cancers17071100.
[27] Khokhlova TD, Canney MS, Khokhlova VA, Sapozhnikov OA, Crum LA, Bailey MR. Controlled tissue emulsification produced by high intensity focused ultrasound shock waves and millisecond boiling. J Acoust Soc Am 2011;130(5):3498–510. doi: 10.1121/1.3626152.
[28] Canney MS, Khokhlova VA, Bessonova OV, Bailey MR, Crum LA. Shock-induced heating and millisecond boiling in gels and tissue due to high intensity focused ultrasound. Ultrasound Med Biol 2010;36(2):250–67. doi: 10.1016/j.ultrasmedbio.2009.09.010.
[29] Khokhlova TD, Monsky WL, Haider YA, Maxwell AD, Wang YN, Matula TJ. Histotripsy liquefaction of large hematomas. Ultrasound Med Biol 2016;42(7):1491–8. doi: 10.1016/j.ultrasmedbio.2016.01.020.
[30] Khokhlova VA, Rosnitskiy PB, Tsysar SA, Buravkov SV, Ponomarchuk EM, Sapozhnikov OA, et al. Initial assessment of boiling histotripsy for mechanical ablation of *ex vivo* human prostate tissue. Ultrasound Med Biol 2023;49:62–71. doi: 10.1016/j.ultrasmedbio.2022.07.014.
[31] Rosnitskiy PB, Tsysar SA, Karzova MM, Buravkov SV, Malkov PG, Danilova NV, et al. Pilot *ex vivo* study on non-thermal ablation of human prostate adenocarcinoma tissue using boiling histotripsy. Ultrasonics 2023;133:107029. doi: 10.1016/j.ultras.2023.107029.
[32] Kumar YN, Singh Z, Wang YN, Kanabolo D, Chen L, Bruce M, et al. A comparative study of histotripsy parameters for the treatment of fibrotic *ex-vivo* human benign prostatic hyperplasia tissue. Sci Rep 2024;14(1):20365. doi: 10.1038/s41598-024-71163-2.
[33] Ponomarchuk E, Tsysar S, Kvashennikova A, Chupova D, Pestova P, Danilova N, et al. Pilot study on boiling histotripsy treatment of human leiomyoma *ex vivo*. Ultrasound Med Biol 2024;50(8):1255–61. doi: 10.1016/j.ultrasmedbio.2024.05.002.
[34] Ponomarchuk EM, Tsysar SA, Chupova DD, Pestova PA, Kvashennikova AV, Danilova NV, et al. Pilot experiment on non-invasive non-thermal disintegration of human mucinous breast carcinoma *ex vivo* using boiling histotripsy. Bull Exp Biol Med 2024;177(1):133–6. doi: 10.1007/s10517-024-06144-6.
[35] Schade GR, Wang YN, Khokhlova TD, May P, Lin DW, Bailey MR, Khokhlova VA. Assessment of boiling histotripsy dose in human *ex vivo* kidneys and renal tumours. Proceedings of the 16th Annual Conference of The International Symposium for Therapeutic Ultrasound; Tel Aviv, Israel, 2016. doi: 10.1186/s40349-016-0079-2
[36] Ponomarchuk E, Tsysar S, Kvashennikova A, Pestova P, Papikyan L, Kadrev A, et al. Non-thermal ultrasound-guided fractionation of human leiomyosarcoma with boiling histotripsy: an *ex vivo* feasibility study. Ultrasonics 2026;159:107876. doi: 10.1016/j.ultras.2025.107876.
[37] Khokhlova TD, Wang YN, Simon JC, Cunitz BW, Starr F, Paun M, et al. Ultrasound-guided tissue fractionation by high intensity focused ultrasound in an *in vivo* porcine liver model. Proc Natl Acad Sci USA 2014;111(22):8161–6. doi: 10.1073/pnas.1318355111.
[38] Khokhlova TD, Schade GR, Wang YN, Buravkov SV, Chernikov VP, Simon JC, et al. Pilot *in vivo* studies on transcutaneous boiling histotripsy in porcine liver and kidney. Sci Rep 2019;9(1):20176. doi: 10.1038/s41598-019-56658-7.
[39] Ponomarchuk E, Thomas G, Song M, Krokhmal A, Kvashennikova A, Wang YN, et al. Histology-based quantification of boiling histotripsy outcomes via ResNet-18 network: towards mechanical dose metrics. Ultrasonics 2024;138:107225. doi: 10.1016/j.ultras.2023.107225.
[40] Ponomarchuk EM, Thomas GPL, Song M, Wang YN, Totten S, Schade GR, et al. Respiratory motion effects and mitigation strategies on boiling histotripsy in porcine liver and kidney. IEEE Trans Ultrason Ferroelectr Freq Control 2025;72(6):837–46. doi: 10.1109/TUFFC.2025.3559458.
[41] Heo J, Joung C, Pahk K, Pahk KJ. Investigation of the long-term healing response of the liver to boiling histotripsy treatment *in vivo*. Sci Rep 2022;12(1):14462. doi: 10.1038/s41598-022-18544-7.

[42] Joung C, Heo J, Pahk KJ, Pahk K. Boiling histotripsy exhibits anti-fibrotic effects in animal models of liver fibrosis. Sci Rep 2024;14(1):15099. doi: 10.1038/s41598-024-66078-x.
[43] Pahk KJ, Mohammad GH, Malago M, Saffari N, Dhar DK. A novel approach to ultrasound-mediated tissue decellularization and intra-hepatic cell delivery in rats. Ultrasound Med Biol 2016;42(8):1958–67. doi: 10.1016/j.ultrasmedbio.2016.03.020.
[44] Chevillet JR, Khokhlova TD, Giraldez MD, Schade GR, Starr F, Wang YN, et al. Release of cell-free microRNA tumor biomarkers into the blood circulation with pulsed focused ultrasound: a noninvasive, anatomically localized, molecular liquid biopsy. Radiology 2017;283(1):158–67. doi: 10.1148/radiol.2016160024.
[45] Schade GR, Wang YN, D'Andrea S, Hwang JH, Liles WC, Khokhlova TD. Boiling histotripsy ablation of renal cell carcinoma in the Eker rat promotes a systemic inflammatory response. Ultrasound Med Biol 2019;45(1):137–47. doi: 10.1016/j.ultrasmedbio.2018.09.006.
[46] Pahk KJ, Shin CH, Bae IY, Yang Y, Kim SH, Pahk K, et al. Boiling histotripsy-induced partial mechanical ablation modulates tumour microenvironment by promoting immunogenic cell death of cancers. Sci Rep 2019;9(1):9050. doi: 10.1038/s41598-019-45542-z.
[47] Eranki A, Srinivasan P, Ries M, Kim A, Lazarski CA, Rossi CT, et al. High-intensity focused ultrasound (HIFU) triggers immune sensitization of refractory murine neuroblastoma to checkpoint inhibitor therapy. Clin Cancer Res 2020;26(5):1152–61. doi: 10.1158/1078-0432.CCR-19-1604.
[48] Hendricks-Wenger A, Hutchison R, Vlaisavljevich E, Allen IC. Immunological effects of histotripsy for cancer therapy. Front Oncol 2021;11:681629. doi: 10.3389/fonc.2021.681629.
[49] Pepple AL, Guy JL, McGinnis R, Felsted AE, Song B, Hubbard R, et al. Spatiotemporal local and abscopal cell death and immune responses to histotripsy focused ultrasound tumor ablation. Front Immunol 2023;14:1012799. doi: 10.3389/fimmu.2023.1012799.
[50] Mouratidis P, Ferreira RC, Anbalagan S, Chauhan R, Rivens I, Ter Haar G. Transcriptomic profiling of the immune response in orthotopic pancreatic tumours exposed to combined boiling histotripsy and oncolytic reovirus treatment. Pharmaceutics 2025;17(8):949. doi: 10.3390/pharmaceutics17080949.
[51] Fiz F, Viganò L, Gennaro N, Costa G, La Bella L, Boichuk A, et al. Radiomics of liver metastases: a systematic review. Cancers (Basel) 2020;12(10):2881. doi: 10.3390/cancers12102881.
[52] Kaloev AZ, Nikolaev DA, Khokhlova VA, Tsysar SA, Sapozhnikov OA. Spatial correction of an acoustic hologram for reconstructing surface vibrations of an axially symmetric ultrasound transducer. Acoust Phys 2022;68(1):71–82. doi: 10.1134/S1063771022010043.
[53] Ponomarchuk EM, Yuldashev PV, Nikolaev DA, Tsysar SA, Mironova AA, Khokhlova VA. Nonlinear ultrasound fields generated by an annular array with electronic and geometric adjustment of its focusing angle. Acoust Phys 2023;69(4):459–70. doi: 10.1134/S1063771023600560.
[54] Yuldashev PV, Karzova MM, Kreider W, Rosnitskiy PB, Sapozhnikov OA, Khokhlova VA. "HIFU Beam:" A simulator for predicting axially symmetric nonlinear acoustic fields generated by focused transducers in a layered medium. IEEE Trans Ultrason Ferroelectr Freq Control 2021;68(9):2837–52. doi: 10.1109/TUFFC.2021.3074611.
[55] Ponomarchuk EM, Rosnitskiy PB, Tsysar SA, et al. Elastic properties of aging human hematoma model *in vitro* and its susceptibility to histotripsy liquefaction. Ultrasound Med Biol 2024;50(6):927–38. doi: 10.1016/j.ultrasmedbio.2024.02.019.
[56] Baumgartner C, Hasgall PA, Di Gennaro F, Neufeld E, Lloyd B, Gosselin MC, Payne D, Klingenböck A, Kuster N. IT'IS database for thermal and electromagnetic parameters of biological tissues. 2025. Version 5.0. https://itis.swiss/virtual-population/tissue-properties/overview.
[57] Duck F. Physical Properties of Tissues: A Comprehensive Reference Book. Cambridge: Academic Press; 1990.
[58] Tran T, Sundaram CP, Bahler CD, Eble JN, Grignon DJ, Monn MF, et al. Correcting the shrinkage effects of formalin fixation and tissue processing for renal tumors: toward standardization of pathological reporting of tumor size. J Cancer 2015;6:759–66. doi: 10.7150/jca.12094.
[59] Ponomarchuk E, Tsysar S, Kadrev A, Kvashennikova A, Chupova D, Pestova P, et al. Boiling histotripsy in *ex vivo* human brain: proof-of-concept. Ultrasound Med Biol 2025;51(2):312–20. doi: 10.1016/j.ultrasmedbio.2024.10.006.
[60] Masuzaki R, Tateishi R, Yoshida H, Sato T, Ohki T, Goto T, et al. Assessing liver tumor stiffness by transient elastography. Hepatol Int 2007;1(3):394–7. doi: 10.1007/s12072-007-9012-7.
[61] Wang YN, Khokhlova TD, Buravkov S, Chernikov V, Kreider W, Partanen A, et al. Mechanical decellularization of tissue volumes using boiling histotripsy. Phys Med Biol 2018;63(23):235023. doi: 10.1088/1361-6560/aaef16.
[62] Zimmermann A. Metastatic liver disease: secondary alterations of hepatic metastases. Tumors and tumor-like lesions of the hepatobiliary tract. Cham: Springer; 2017. doi: 10.1007/978-3-319-26956-6_109.
[63] Ponomarchuk EM, Rosnitskiy PB, Khokhlova TD, Buravkov SV, Tsysar SA, Karzova MM, et al. Ultrastructural analysis of volumetric histotripsy bio-effects in large human hematomas. Ultrasound Med Biol 2021;47(9):2608–21. doi: 10.1016/j.ultrasmedbio.2021.05.002.
[64] Yu Z, Xu C, Song B, Zhang S, Chen C, Li C, et al. Tissue fibrosis induced by radiotherapy: current understanding of the molecular mechanisms, diagnosis and therapeutic advances. J Transl Med 2023;21(1):708. doi: 10.1186/s12967-023-04554-0.
[65] Dagher OK, Schwab RD, Brookens SK, Posey Jr AD. Advances in cancer immunotherapies. Cell 2023;186(8):1814.e1. doi: 10.1016/j.cell.2023.02.039.
[66] Qu S, Worlikar T, Felsted AE, Ganguly A, Beems MV, Hubbard R, et al. Non-thermal histotripsy tumor ablation promotes abscopal immune responses that enhance cancer immunotherapy. J Immunother Cancer 2020;8(1):e000200. doi: 10.1136/jitc-2019-000200.
[67] Eranki A, Srinivasan P, Ries M, Kim A, Lazarski CA, Rossi CT, et al. High-intensity focused ultrasound (HIFU) triggers immune sensitization of refractory murine neuroblastoma to checkpoint inhibitor therapy. Clin Cancer Res 2020;26(5):1152–61. doi: 10.1158/1078-0432.CCR-19-1604.
[68] Mouratidis PXE, Costa M, Rivens I, Repasky EE, Ter Haar G. Pulsed focused ultrasound can improve the anti-cancer effects of immune checkpoint inhibitors in murine pancreatic cancer. J R Soc Interface 2021;18(180):20210266. doi: 10.1098/rsif.2021.0266.
[69] Dmello RS, To SQ, Chand AL. Therapeutic targeting of the tumour microenvironment in metastatic colorectal cancer. Int J Mol Sci 2021;22(4):2067. doi: 10.3390/ijms22042067.
[70] Zhu C, Liao JY, Liu YY, Chen ZY, Chang RZ, Chen XP, et al. Immune dynamics shaping pre-metastatic and metastatic niches in liver metastases: from molecular mechanisms to therapeutic strategies. Mol Cancer 2024;23(1):254. doi: 10.1186/s12943-024-02171-z.
[71] de Ridder J, de Wilt JH, Simmer F, Overbeek L, Lemmens V, Nagtegaal I. Incidence and origin of histologically confirmed liver metastases: an explorative case-study of 23,154 patients. Oncotarget 2016;7(34):55368–76. doi: 10.18632/oncotarget.10552.
[72] Karpov OE, Vetshev PS, Bruslik SV, Sviridova IT, Bruslik DS. Non-invasive high-intensity focused ultrasound ablation of secondary liver tumors. Med J Dr Ru 2015;1(11):37–41.
[73] Khokhlova TD, Haider YA, Maxwell AD, Kreider W, Bailey MR, Khokhlova VA. Dependence of boiling histotripsy treatment efficiency on HIFU frequency and focal pressure levels. Ultrasound Med Biol 2017;43(9):1975–85. doi: 10.1016/j.ultrasmedbio.2017.04.030.
[74] Thomas GPL, Khokhlova TD, Sapozhnikov OA, Wang YN, Totten SI, Khokhlova VA. In vivo aberration correction for transcutaneous HIFU therapy using a multielement array. IEEE Trans Ultrason Ferroelectr Freq Control 2022;69(10):2955–64. doi: 10.1109/TUFFC.2022.3200309.
[75] de Greef M, Schubert G, Wijlemans JW, Koskela J, Bartels LW, Moonen CTW, et al. Intercostal high intensity focused ultrasound for liver ablation: the influence of beam shaping on sonication efficacy and near-field risks. Med Phys 2015;42(8):4685–97. doi: 10.1118/1.4925056.
[76] Tsang SH, Ma KW, She WH, Chu F, Lau V, Lam SW, et al. High-intensity focused ultrasound ablation of liver tumors in difficult locations. Int J Hyperthermia 2021;38(2):56–64. doi: 10.1080/02656736.2021.1933217.
[77] Knott EA, Longo KC, Vlaisavljevich E, Zhang X, Swietlik JF, Xu Z, et al. Transcostal histotripsy ablation in an in vivo acute hepatic porcine model. Cardiovasc Intervent Radiol 2021;44(10):1643–50. doi: 10.1007/s00270-021-02914-1.
[78] Kisting MA, White JK, Periyasamy S, Kutlu AZ, Kisting AL, Zhang X, et al. Safety and efficacy of histotripsy delivery through overlying gas-filled small bowel in an *ex vivo* swine model. Int J Hyperthermia 2024;41(1):2369305. doi: 10.1080/02656736.2024.2369305.
[79] Rosnitskiy PB, Yuldashev PV, Sapozhnikov OA, Gavrilov LR, Khokhlova VA. Simulation of nonlinear trans-skull focusing and formation of shocks in brain using a fully populated ultrasound array with aberration correction. J Acoust Soc Am 2019;146:1786. doi: 10.1121/1.5126685.
[80] Rosnitskiy PB, Khokhlova TD, Schade GR, Sapozhnikov OA, Khokhlova VA. Treatment planning and aberration correction algorithm for HIFU ablation of renal tumors. IEEE Trans Ultrason Ferroelectr Freq Control 2024;71(3):341–53. doi: 10.1109/TUFFC.2024.3355390.
[81] Rosnitskiy PB, Thomas GPL, Lee GL, Khokhlova VA, Sapozhnikov OA, Schade GR, et al. A fully populated transrectal array for boiling histotripsy ablation of the prostate. IEEE Trans Ultrason Ferroelectr Freq Control 2025. doi: 10.1109/TUFFC.2025.3596780.